Biogeosciences Discuss., 4, 2179–2213, 2007
www.biogeosciences-discuss.net/4/2179/2007/

Biogeosciences
Discussions

Early diagenetic overprint in Caribbean sediment cores and its effect on the geochemical composition of planktonic foraminifera

M. Regenberg[1], **D. Nürnberg**[1], **J. Schönfeld**[1], **and G.-J. Reichart**[2]

[1]Leibniz Institute of Marine Sciences IFM-GEOMAR, Kiel, Germany
[2]Faculty of Earth Sciences, Utrecht University, The Netherlands

Received: 7 June 2007 – Accepted: 14 June 2007 – Published: 4 July 2007

Correspondence to: M. Regenberg (mregenberg@ifm-geomar.de)

Abstract

Early diagenetic features are noticed in the vicinity of carbonate platforms. Planktonic foraminifera of two tropical Atlantic deep-sea sediment cores show the strict relation between micro-scale euhydral crystallites of inorganic precipitates, higher oxygen isotope values and Mg/Ca ratios, and lower Sr/Ca ratios than expected for their pelagic environment in the time interval of ~100 000–550 000 calendar years before present. Laser ablation Mg/Ca (Sr/Ca) of crystallite-bearing foraminiferal chamber walls revealed 4–6 times elevated (2–3 times depleted) ratios, when ablating the diagenetic overgrowth. Crystalline overgrowth in proportions of 10–20% are estimated to cause the observed geochemical alteration. The extent of foraminiferal Mg/Ca alteration, moreover, seems to be controlled by the composition of the bulk sediment, especially the content of high-magnesium calcite. Anomalous ratios of >6 mmol/mol only occur, when high-magnesium calcite has dissolved within the sediment. The older parts (back to ~800 kyrs) of the records are characterized by similar trends of Mg/Ca and Sr/Ca. We discuss possible scenarios to accommodate the obtained geochemical information.

1 Introduction

A persistent problem in many paleoceanographic studies is the potential of diagenetic processes to compromise the fidelity of geochemical proxies in deep-sea carbonates and microfossils, such as foraminifera. Principally, two processes of deep-sea carbonate diagenesis can be distinguished from each other: first, the geochemical composition may be biased by dissolution processes on the sediment's carbonate mineralogy (e.g., Droxler, 1984; Sabine and Mackenzie, 1995; Haddad and Droxler, 1996; Malone et al., 2001; Frank and Bernet, 2000; Jansen et al., 2002), and on the foraminiferal isotope and element content (e.g., Lorens et al., 1977; Lohmann, 1995; Rosenthal et al., 1997; Dekens et al., 2002; Regenberg et al., 2006). Second, the geochemical composition may be altered by precipitation and reprecipitation of calcite from sediment pore fluid (e.g., Baker et al., 1982; Norris and Wilson, 1998; Hover et al., 2001; Rudnicki et al., 2001). Dissolution and/or inorganic reprecipitation is determined by the saturation state of seawater or pore fluid with respect to the solid phase (e.g., Morse, 2003; Funk et al., 2003; Regenberg et al., 2006). Inorganic (or diagenetic) calcite in terms of overgrowth may mask the primary oceanographic signal of planktonic foraminiferal tests. Both, inorganic calcite overgrowth and dissolution of foraminiferal tests during shallow burial tend to bias the oxygen isotope composition (δ^{18}O) to more positive values (Killingley, 1983; Mulitza et al., 2004).

A paramount aim of geochemical studies focussing on diagenetic issues is quantification of the alteration. One strategy for quantifying the extent of diagenesis is the application of numerical models to assess pore-fluid and precipitate isotope compositions (e.g., Killingley, 1983; Richter and DePaolo, 1987; Schrag et al., 1992; Schrag, 1999; Rudnicki et al., 2001). Basically, these studies address deep-buried sediments from depths of >300 m. Another approach for the quantification of diagenetic alteration deals with the Element/Ca ratios and their alignment to measured pore-fluid composition by application of partition coefficients (e.g., Tripati et al., 2003; Sexton et al., 2006).

Here, we found unexpected diagenetic overprint in shallow-buried sediments in tropical Atlantic and Caribbean deep-sea cores from different water depths (~1700–2700 m; Fig. 1) marginally described before (Müller, 1999). We applied oxygen isotope and Element/Ca analysis on bulk planktonic foraminiferal tests revealing anomalous ratios compared to established data sets reflecting past environmental conditions. Since information on the bulk foraminiferal geochemical composition altered by diagenesis combines the actual biogenic calcite signal and the composition of the inorganic precipitate, we additionally performed laser ablation inductively coupled plasma mass spectrometry capable to generate high resolution Element/Ca-ratio profiles of foraminiferal tests (Eggins et al., 2003; Hathorne et al., 2003; Reichart et al., 2003). This technique allows to determine end-member compositions of the diagenetic precipitates. Associated carbonate mineralogy of the bulk sediment affords the possibility to characterize the processes involved in sediment alteration.

2 Materials and methods

Piston cores SO164–07–4 and SO164–19–2 were recovered during R/V SONNE cruise 164 (Nürnberg et al., 2003) from Windward Passage (21°19′27.6″ N, 74°08′46.2″ W at 2722 m and 21°14′42.6″ N, 74°20′59.4″ W at 1704 m, respectively (Fig. 1)). Syringe sampling (∼10 mL) of the upper ∼9.5 m of site SO164–07–4 and ∼6.5 m of site SO164–19–2, respectively, took place every 5 cm. Samples taken from the ∼2.2 m of intercalated calcite-turbidite sequences of site SO164–07–4 were discarded.

2.1 Analysis of carbonate phases

The relative abundance of a variety of minerals present in the sediment samples was quantified by X-ray diffraction (XRD). XRD was typically performed on ∼0.5 g of the bulk sediment. Each sample was carefully grinded for five minutes in an agate mortar in order to homogenize the grain size to ∼5–10 μm. The analysis was carried out on a Philips PW 1710 X-ray diffractometer (IFM-GEOMAR, Kiel) containing a cobalt anode Kσ tube at 40 KV and 35 mA. The samples were scanned from 25–40° at a scanning speed of 0.01 steps per second to cover the significant peaks of the various carbonate minerals. The peak-area method was deployed to quantify the aragonite content using the computer based integration program MacDiff of Petschick (2001). The aragonite/calcite peak-area ratios were converted into relative weight percentages using an in-house calibration curve. Weight percentages of HMC and LMC were directly calculated by their peak-area ratios.

2.2 $\delta^{18}O$ analysis

For stable isotope analysis, 10 specimens of planktonic foraminifera *Globigerinoides sacculifer* (without sac-like final chamber) were selected from the 315–400 µm size fraction. All isotope analyses were run on a Finnigan MAT 252 Mass Spectrometer with automated Kiel carbonate preparation device at IFM-GEOMAR (Kiel). The mass spectrometer was calibrated via the National Bureau of Standards (NBS) 19 and an internal laboratory standard to the Vienna Pee Dee Belemnite (PDB) scale. Isotope values are reported in ‰ PDB. The external reproducibility of in-house carbonate standards was ~0.08‰ for $\delta^{18}O$.

2.3 Element/Ca analysis

Twenty to twenty-five specimens (~550–800 µg) of *Globigerinoides ruber* white, *G. sacculifer* (without sac-like final chamber), and *Neogloboquadrina dutertrei* were selected from the 315–400 µm size fraction. Clay removal (water and methanol wash) and organic-matter oxidation (hydrogen peroxide treatment) were applied to gently crushed samples, followed by a weak acid leach and final dissolution of the fragments. For detailed description of the Mg-cleaning protocol (Barker et al., 2003), see Regenberg et al. (2006).

Element/Ca ratios were performed on two inductively coupled plasma optical emission spectrometry (ICP OES) devices showing no significant offsets in Mg/Ca (Regenberg et al., 2006). All *G. sacculifer* samples, and parts of the *G. ruber* w. and *N. dutertrei* samples, were analyzed on an ICP OES (ISA Jobin Yvon, Spex Instruments S.A. GmbH) at IFM-GEOMAR, Kiel, using yttrium (10 ppm) as internal standard. Relative analytical errors for calcium and strontium were ~0.15%, for magnesium ~0.45%, for manganese ~10%, and for iron ~15%. The remainder of the *G. ruber* w. and *N. dutertrei* samples were measured on an ICP OES (Spectro CirosCCD SOP) at the Institute for Geosciences, Kiel. Relative analytical errors for Mg/Ca and Sr/Ca ratios were ~0.1%. For manganese and iron, analytical errors amount to ~0.5% and

∼2%, respectively.

2.4 Chronostratigraphy

The stratigraphical framework for the upper ∼9.5 m (including ∼2.2 m of turbidite sediment) of site SO164–07–4 (Fig. 2) was established by graphically correlating prominent maxima and minima in the planktonic oxygen isotope record of *G. sacculifer* to the stacked reference curve of Martinson et al. (1987).The age model for the upper ∼6.5 m of site SO164–19–2 (Fig. 2) is based on the graphic correlation of the magnetic susceptibility curve younger than ∼290 ka with the stacked reference curve of Martinson et al. (1987). For graphical correlation back to ∼820 kyrs, the magnetic susceptibility curve was correlated to the benthic isotope record of ODP Site 677 (Shackleton et al., 1990). Definition of marine isotope stages (MIS) follows Bassinot et al. (1994), graphic correlation was performed with AnalySeries Version 1.1 (Paillard et al., 1996). To further constrain the chronostratigraphy of site SO164–19–2, we studied the presence/absence of the planktonic foraminifera *Globorotalia menardii*, serving as time stratigrahic markers and climatic indicators in Pleistocene sediments from the tropical Atlantic (Ericson and Wollin, 1956, 1968; Ruddiman, 1971). Abundance peaks and barren zones correspond, to some extent, with warm and cold marine isotopic stages, respectively (Fig. 2).

2.5 LA-ICP MS

For laser ablation inductively coupled plasma mass spectrometry (LA-ICP MS), we selected cleaned *G. ruber* w., *G. sacculifer*, and *N. dutertrei* fragments from the 315–400 μm size fraction of five different samples. Multiple laser ablation profiles were performed on different foraminiferal fragments from the same sample to elucidate intest heterogeneities. In total, 18 profiles were ablated.

Using an Excimer 193 nm deep ultra violet laser (Lambda Physik) with Geolas optics (Günther et al., 1997), craters of 80 μm in diameter were ablated during analysis. Energy density at the sample surface was kept at 2 mJ/cm^2, shot repetition rate at 8 Hz. Laser ablation of calcite requires ablation at ultra violet wave lengths since higher wave lengths result in uncontrolled cleavage. The ablated material was transported on a continuous He flow and mixed with an Ar make up gas before injection into the Ar plasma of the quadrupole ICP MS instrument (Micromass Platform at the Faculty of Geosciences, Utrecht University, Netherlands). A collision and reaction cell was used to improve results by reducing spectral interferences on the minor isotopes of Ca (^{42}Ca, ^{43}Ca, and ^{44}Ca). Interelemental fractionation was insignificant due to the relative low depth to width ratio of the ablation craters produced (Mason and Mank, 2001). The use of a collision cell also prevented interference of clusters like ^{12}C^{16}O^{16}O. Although the Excimer UV-193 usually does not show any matrix effects, possible matrix effects, nevertheless, were checked with matrix matched in-house standards. Calibration was performed against U.S. National Institute of Standards and Technology SRM 612 glass using the concentration data of Pearce et al. (1997), with Ca as an internal standard. Calcium carbonate is well suited for LA-ICP MS because Ca can be used as an internal standard at 40 weight percentages. We used ^{44}Ca for quantification, ^{42}Ca and ^{43}Ca for internal monitoring. Using Ca as an internal standard allows direct comparison to trace metal to Ca ratios from traditional wet-chemical studies. Concentrations of Mg and Sr were calculated using ^{24}Mg and ^{26}Mg, and ^{88}Sr. Although the accuracy for the more abundant ^{24}Mg is higher, both Mg isotopes agree within a few percent.

With initiation of the ablation process, preferential ablation of material from surfaces that lie orthogonal to the incident laser beam results in greater ablation from the tops of interpore ridges and spine bases (Eggins et al., 2003). This means that the ablation crater is not flat but follows the curvature of the foraminiferal test, and, therefore, should reveal elevated element concentrations in a diagenetic coating when present. Further in the ablation process the craters become increasingly flatter bottomed. This results in a smoothing of the signal when the ablation reaches the pores on the other side of the test. To certify that no smoothing of a possible coating peak occurred, the fragments of each sample were measured both from the inner side toward the outer side and vice versa.

3 Results

3.1 Carbonate mineralogy

The composition of the bulk-sediment carbonate of sites SO164–19–2 and SO164–07–4 changes through time (Fig. 3). For site SO164–19–2, the content of HMC (with Mg^{2+} concentrations >4 mol.% (Morse, 2003)) on the carbonate phases amounts to 6–12% from the core top back until ~140 kyrs with an additional peak at ~220 kyrs. From the core top back until ~270 kyrs, aragonite contributes with 50–60% to the carbonate content. A marked decrease leads to the absence of aragonite (and HMC) from the sediments prior to ~300 kyr, except for two aragonite peaks at ~280 kyrs and ~410–420 kyrs. Higher resolution site SO164–07–4 shows the permanent presence of aragonite and HMC from the core top back until ~48 kyrs at 40–70% and 7–12%, respectively. Further back to ~116 kyrs, HMC is present in most of the samples in proportions of 8–21%, while aragonite is only present at ~85 kyrs. Prior to ~116 kyrs, HMC is absent except for the time interval of ~139–149 kyrs. From ~131–169 kyrs, aragonite is only present in single peaks, whereas prior to ~169 kyrs, aragonite is permanent present in proportions of 16–52%.

3.2 $\delta^{18}O$, Mg/Ca, and Sr/Ca records of sites SO164–19–2 and SO164–07–4

The $\delta^{18}O$, Mg/Ca, and Sr/Ca records of sites SO164–19–2 and SO164–07–4 reveal atypical patterns compared to proxy records from the same area available in the literature. Site SO164–19–2 covers the glacial/interglacial cycles back to ~820 kyrs in low resolution (Fig. 4). Core top, Holocene, and interglacial isotope stage $\delta^{18}O$ values are consistent with the corresponding values of site SO164–07–4. Reaching values as high as 1.62‰ and prior to MIS 3 not lower than about −0.5‰, $\delta^{18}O$ is far offset from the Caribbean ODP Site 999 $\delta^{18}O$ record of *G. ruber* w. (Schmidt et al., 2006) showing highest values of ~0.1‰ during MIS 2 and MIS 12 (Fig. 4). From MIS 14–20, variation in δ^{18}O is considerably dampened, values are around 0.5‰.

Mg/Ca ratios of site SO164–19–2 show a completely different trend compared to the *G. ruber* w. record of ODP Site 999 (Schmidt et al., 2006). Expected lower Mg/Ca during MIS 2–4 with respect to core-top and Holocene ratios are not observed (Fig. 4). From *G. ruber* w. Mg/Ca of ~5.5 mmol/mol during this time interval and throughout MIS 5, an intense increase to ratios >8 mmol/mol occurs during MIS 6. Among a hugh variability of ~3 mmol/mol, Mg/Ca further increases to >10 mmol/mol during MIS 10–12. This trend is also reflected in the Mg/Ca records of *G. sacculifer* and *N. dutertrei* of site SO164–19–2 (Fig. 4), whereas the latter is almost constantly offset by ~2.5–3 mmol/mol to lower ratios. Decreasing Mg/Ca particularly during MIS 13 level off the ratios of *G. sacculifer* to ~6–7 mmol/mol during MIS 16–18. Lower ratios than core-top Mg/Ca are observed for MIS 20. Comparing the younger part of the record to the *G. sacculifer* Mg/Ca of site SO164–07–4, a similar trend at least during MIS 5 and MIS 7 to the *G. sacculifer* and *G. ruber* w. records of site SO164–19–2 can be seen (Fig. 4).

G. sacculifer Sr/Ca ratios of ~1.4 mmol/mol are observed back until MIS 7 with excursions to ~1.3 mmol/mol during MIS 6. A similar trend is shown by the *G. sacculifer* Sr/Ca curve of site SO164–07–4. During MIS 8, Sr/Ca decreases to ratios of ~1.25–1.3 mmol/mol. This level persists until MIS 14 with excursions to minimum ratios of ~1.2 mmol/mol. During MIS 14, Sr/Ca decreases to a level of ~1.2 mmol/mol. In the oldest parts, Sr/Ca further decreases to ratios <1 mmol/mol. For the entire record, Sr/Ca of *G. ruber* w. and *N. dutertrei* of site SO164–19–2 are offset to higher ratios by ~0.5–1 mmol/mol and follow the trend of *G. sacculifer*. The decreasing trend in all planktonic foraminiferal Sr/Ca records prior to MIS 6 contradicts the *G. ruber* w. Sr/Ca record of site MD02–2575 from the Gulf of Mexico (data obtained from C. Karas and D. Nürnberg, personal communication), which remains at the same level of ~1.4–1.5 mmol/mol from MIS 6–11.

3.3 Atypical trends in Caribbean δ^{18}O and Mg/Ca records

The *G. sacculifer* δ^{18}O record of site SO164–07–4 shows two complete glacial cycles back to MIS 8 at ~270 kyrs (Fig. 2, 5). δ^{18}O values across Terminations I and II display glacial/interglacial differences of ~2.2‰ and ~1.6‰, respectively. Other (sub)tropical Atlantic, Caribbean, and Bahamian records (Curry and Oppo, 1997; Wolff et al., 1998; Rühlemann et al., 1999; Kroon et al., 2000; Schmidt et al., 2004, 2006), in contrast, indicate that differences across both terminations are similar. The difference across Termination III of ~1.2‰ better matches with the range of ~1.1‰ observed for Caribbean ODP Site 999 (Schmidt et al., 2006) (Fig. 5). The Holocene attains minimum δ^{18}O of about −1.5‰, which is exceeded in interglacial MIS 5 and MIS 7 with values of about −1.0‰ and −0.5‰, respectively. In contrast to other studies (Kroon et al., 2000; Schmidt et al., 2006), the Holocene stands out in the record with the most negative δ^{18}O values. Highest values during glacial MIS 2, MIS 6, and MIS 8 are close to 0.9‰. In lower resolution, the *G. sacculifer* δ^{18}O records of sites M35027 and M35053 (Müller, 1999) go back to MIS 5, with more depleted Holocene values than site SO164–07–4, but with similar increased values during MIS 5 (Fig. 5).

Mean Holocene *G. sacculifer* Mg/Ca ratios yield ~4.5 mmol/mol (Fig. 5). These Mg/Ca ratios correspond to reasonable temperatures of ~27.0°C, when applying the species-specific paleotemperature equation of Anand et al. (2003). Mg/Ca of site SO164–07–4 decreases to ~3.7 mmol/mol (~24.4°C) during the Last Glacial Maximum (LGM, 18–24 kyr). This Holocene/LGM change in Mg/Ca of ~0.8 mmol/mol is consistent with previous estimates for the Caribbean (Hastings et al., 1998; Schmidt et al., 2004, 2006). From the Holocene to MIS 3, Mg/Ca of site SO164–07–4 is nearly parallel offset by ~0.2 mmol/mol from the *G. ruber* w. record of Caribbean ODP Site 999 (Schmidt et al., 2004, 2006). Prior to MIS 4, Mg/Ca reveals lowest values of ~5 mmol/mol. From this level, Mg/Ca increases to as much as 6.66 mmol/mol during MIS 5e and 7.13 mmol/mol during MIS 7, corresponding to temperatures of ~32.2°C and ~33.1°C, respectively. Prior to MIS 4, Mg/Ca diverges from the ratios of ODP

Site 999 (Schmidt et al., 2006). During MIS 5, MIS 6, and late MIS 7, the offset amounts to ~1.5–2 mmol/mol, increasing to ~3 mmol/mol for the oldest parts. The Mg/Ca records of sites M35027 and M35053 (Müller, 1999) generally show the same atypical trend like those of site SO164–07–4. In general, the downcore increasing trend in δ^{18}O, obviously for the interglacials, is synchronized to the increasing trend in Mg/Ca (Fig. 5).

3.4 Negligible influence of contaminating phases on Mg/Ca ratios

With respect to the Mg/Ca and Sr/Ca ratios of tropical Atlantic and Caribbean sediment-surface samples (Regenberg et al., 2006), downcore records of sites SO164–07–4 and SO164–19–2 reveal elevated Mg/Ca and lowered Sr/Ca (Fig. 6a). To evaluate the possible contribution of contaminating phases high in magnesium, iron, and/or manganese (i.e. clay minerals, Mn-oxide coatings) to the original planktonic foraminiferal Mg/Ca and Sr/Ca, we measured the Fe/Ca and Mn/Ca ratios of our foraminiferal sample solutions. These phases may coat or adhere to the surfaces of tests. Barker et al. (2003) found Fe/Ca and Mn/Ca of around 0.2 mmol/mol and 0.1 mmol/mol, respectively, typically for foraminiferal tests devoid of contaminating phases. These ratios, which imply negligible elevation of Mg/Ca, are observed for the sediment-surface and site SO164–19–2 samples (Fig. 6b). For site SO164–07–4, elevated foraminiferal Mn/Ca of up to 0.6 mmol/mol may be indicative of contamination by Mn-oxide coatings. The suggested contribution of Mg^{2+} from coatings to the foraminiferal Mg/Ca of ~1% (Barker et al., 2003), however, cannot account alone for the atypically high Mg/Ca (up to 7.13 mmol/mol) of site SO164–07–4 (Fig. 6a).

3.5 Micro-scale crystallites on planktonic foraminiferal tests

In order to understand the geochemical composition of the planktonic foraminiferal tests atypically for open-ocean conditions (Figs. 4, 5, 6a), we prepared scanning electron microscope (SEM) images of selected cleaned and uncleaned fragments of specimens revealing typical Mg/Ca ratios and anomalously high Mg/Ca, respectively. Tests of those specimens revealing typical Mg/Ca (Figs. 7a, c) show inner and outer chamber-wall surfaces of well preserved biogenic texture with smooth surfaces, wide pores, and well defined outer ridges. In contrast, surfaces of those specimens revealing anomalously high Mg/Ca (Fig. 7) are overgrown with micro-scale euhydral crystallites of secondary precipitates, which cover the outer ridges and fill the pores. The diagenetic overgrowth covers the inner surface even after the intense Mg-cleaning procedure. SEM images of chamber-wall cross sections of specimens without overgrowth display the microgranular texture that is characteristic of biogenic calcite. The intact wall structure comprises wide pores reaching throughout the wall and smooth inner surfaces (Figs. 8a, c). Chamber-wall cross sections of specimens with overgrowths reveal that the crystallites narrow the pores and almost close them at their insides (Fig. 8). Figure 8b displays an uncleaned fragment identifying the diagenetic crystallites as distinct rims with a sharply bordered contact to the biogenic calcite.

3.6 Geochemical composition of the diagenetic overgrowth

To further constrain the possible influence of the crystallites on the planktonic foraminiferal geochemistry, we analyzed the elemental composition of foraminiferal chamber walls of site SO164–19–2 applying LA-ICP MS. Since single laser pulses remove only a few nanometers of material the ablation results in a high resolution profile. We observed a significant different Mg/Ca and Sr/Ca signal for the outermost proportions compared to the remainder of the chamber walls (Fig. 9). Whether close to the inner or outer surfaces, Mg/Ca ratios are 4–6 times elevated and Sr/Ca 2–3 times depleted with respect to the profile averages. For the time interval of ∼260–470 kyrs, chamber-wall surface Mg/Ca is at least 10 mmol/mol (highest observed ratios are >40 mmol/mol; Fig. 9), Sr/Ca shows relatively uniform ratios of ∼0.5–0.8 mmol/mol (Fig. 10).

4 Discussion

The δ^{18}O, Mg/Ca, and Sr/Ca records of downcore planktonic foraminiferal samples of sites SO164–07–4 and SO164–19–2 show to some extent atypical values with respect to previously published data sets reflecting past environmental conditions (Figs. 4, 5). Within the same samples, δ^{18}O values as well as Mg/Ca ratios are higher than expected, Sr/Ca, contrarily, shows the inverse trend with lower ratios than expected.

In principal, the oxygen isotope composition of the actual planktonic foraminiferal test is determined by the composition and (higher) temperature of the pelagic waters, in which the calcite was formed. Since precipitation of the overgrowth during diagenesis is expected to occur near the sediment/bottom-water interface and its oxygen isotope composition is driven by thermodynamic fractionation (e.g., O'Neil et al., 1969; Kim and O'Neil, 1997), δ^{18}O tends to more positive values (e.g., Killingley, 1983; Schrag et al., 1995; Crowley and Zachos, 2000; Pearson et al., 2001; Wade and Kroon, 2002). Like in this study, higher than expected foraminiferal δ^{18}O values from deep-sea sites in conjunction with diagenetic crystalline overgrowth have been observed, yet merely for sample material from great sediment-burial depth (e.g., Pearson et al., 1997; Norris and Wilson, 1998; Price et al., 1998; Wade and Kroon, 2002; Tripati et al., 2003; Sexton et al., 2006).

The common approach to understand the contribution to the calcite composition derived from inorganic precipitates is using downcore pore-fluid data for the calculation and numerical modeling of theoretical precipitate compositions (e.g., Killingley, 1983; Schrag et al., 1992; Schrag, 1999; Rudnicki et al., 2001; Tripati et al., 2003; Sexton et al., 2006). In contrast to these studies, we attempt to quantify the influence of the diagenetic overgrowth with the results from laser-ablation analysis, as downcore pore fluid data are not available for the presented sites and the fluid behavior at the very shallow burial depth of the deep-sea sediments is hardly understood (e.g., Mullins et al., 1985; Morse, 2003).

4.1 Mg/Ca and Sr/Ca data: Assessing the extent of diagenetic alteration

Considering the visual evidence for diagenetic alteration of planktonic foraminiferal tests (Figs. 7, 8) in combination with the results of the laser ablation (Figs. 9, 10), the anomalously high Mg/Ca ratios are best explained by the presence of inorganic calcite: The outermost measurements, even if time-resolved, closely correspond with the outermost position of the diagenetic crystallites. Inorganic calcite contains about an order of magnitude more Mg^{2+} than planktonic foraminiferal calcite (e.g., Katz, 1973; Baker et al., 1982; Mucci and Morse, 1983; Mucci, 1987). We detected 10–40 mmol/mol for the crystallites, typically <7 mmol/mol for the actual test (Fig. 9, 10). Thus, only a limited amount of overgrowth remaining on the foraminiferal test after the Mg-cleaning procedure, would be sufficient to raise the ratio of foraminiferal sample calcite.

Sr/Ca ratios of the ablated chamber-wall cross sections reveal 2–3 times depleted ratios for the inorganic crystallites, which is ~0.5–0.8 mmol/mol. Depending on the species, typical ratios of planktonic foraminifera without overgrowth are in the order of 1.2–1.7 mmol/mol (Fig. 6). Since biogenic calcite contains significantly more Sr^{2+} than inorganic (Baker et al., 1982; Carpenter and Lohmann, 1992), lower Sr/Ca indicates larger proportions of secondary inorganic calcite (Bralower et al., 1997).

In order to estimate the proportion of diagenetic overgrowth necessary to alter the Mg/Ca and Sr/Ca ratios of the actual foraminiferal test by degrees indicated by the downcore records (Fig. 4), we applied a mass balance. End-member phases are an assumed planktonic foraminifera with Mg/Ca of 4 mmol/mol and Sr/Ca of 1.4 mmol/mol, roughly appropriate for interglacial *G. sacculifer*, and three possible Mg/Ca (10, 20, 40 mmol/mol) and two possible Sr/Ca signals (0.5, 0.8 mmol/mol) for the overgrowth, obtained from laser ablation (Table 1). We suggest that a proportion of 10–20% of crystallites is sufficient to increase (decrease) the Mg/Ca (Sr/Ca) the way we observed for sites SO164–07–4 (~7 mmol/mol; Fig. 5) and SO164–19–2 back until MIS 13 (~11 mmol/mol; Fig. 4).

Prior to MIS 13, this straightforward interrelationship between Mg/Ca ratios and

Sr/Ca is not visible anymore, both show similar trends with an intense decrease from MIS 18–20. The recorded δ^{18}O trend during this time interval with values around 0.5‰ and lack of considerable changes implies that the original planktonic foraminiferal signal has almost completely been overprinted or recrystallized. It might be speculated that the system for pore fluid changes the way that dissolution and reprecipitation of carbonate has taken place, which results in increased Sr^{2+} and Mg^{2+} concentrations of coexisting pore fluids (Schrag et al., 1995). A diffusive flux of ions out the top of the sediment column (Schrag et al., 1995) might have depleted the pore fluid (and elevated the overlying fluids). Such carbonate recrystallization is suggested to have relatively minor effects on δ^{18}O values of pore fluid (Schrag et al., 1992).

4.2 Control of high-magnesium calcite on Mg/Ca ratios?

Aragonite and high-magnesium calcite (HMC) get important in areas around carbonate platforms, which distribute these shallow-water carbonates even down to the deep sea (Morse, 2003). Relatively high proportions of aragonite and HMC (Fig. 3) seem to confirm a recent influence of carbonate production on platforms (i.e. most likely the Bahama platform) on the deep-sea region of the presented sites. Nevertheless, reported aragonite production on the Bahama platform and export towards the deeper basins around the platform during sea-level highstands (Kroon et al., 2000; Rendle et al., 2000; Slowey et al., 2002), possibly mirrored in the aragonite contents of site SO164–07–4, are certainly not reflected in the downcore trend of the carbonate phases of shallow site SO164–19–2. Moreover, absence of aragonite and HMC in sediments of site SO164–19–2 prior to ~300 kyrs may result from selective dissolution of both phases, which was observed for deeper water (>1000 m) Bahamian periplatform slope sediments (Mullins et al., 1985; Haak and Schlager, 1989). Associated reprecipitation of low-magnesium calcite in the respective sediments (Mullins et al., 1985) in combination with possible supply of Mg^{2+} through diffusive flux of ions (Schrag et al., 1995) from the deeper sediment column could provide a source to alter the planktonic foraminiferal geochemical composition to the observed extent. Probably, this is why planktonic foraminiferal Mg/Ca ratios and HMC content of sites SO164–07–4 and SO164–19–2 reveal negatively correlated trends (Fig. 11) with occurrence of anomalously high Mg/Ca above ~6 mmol/mol, only when HMC is absent from the sediments.

5 Conclusions

Planktonic foraminiferal δ^{18}O, Mg/Ca, and Sr/Ca records of two deep-sea sediment cores (SO164–07–4, 2722 m; SO164–19–2, 1704 m) from tropical Windward Passage of the last glacial/interglacial cycles reveal values atypical for pelagic environmental conditions. Contemporaneously, δ^{18}O values and Mg/Ca ratios are higher than expected, Sr/Ca shows lower ratios than expected. Contamination by Mg^{2+}-bearing Mn-oxide coatings and clay have been ruled out by considerably low foraminiferal Mn/Ca and Fe/Ca ratios.

Scanning electron microscope images display distinct micro-scale euhydral crystallites of inorganic precipitates on tests with the atypical geochemical composition. Laser ablation measurements of foraminiferal chamber walls identified significant different Mg/Ca (4–6 times elevated) and Sr/Ca signals (2–3 times depleted) for the inorganic precipitates in comparison with the actual foraminiferal test.

Back until marine isotope stage 13, crystalline overgrowth proportions of 10–20%, which cannot by removed by the cleaning procedure applied for foraminiferal Mg/Ca analysis, are sufficient to alter the Mg/Ca and Sr/Ca of the foraminiferal sample calcite to the observed extent. The absence of aragonite and high-magnesium calcite in the sediments prior to ~300 kyrs is likely coupled to selective dissolution within the sediments. It might be speculated that the combined processes of dissolution of these two phases and reprecipitation of low-magnesium calcite contributes as a source for diagenetic alteration of the planktonic foraminiferal geochemical composition. Considering changed interrelationships between the planktonic foraminiferal geochemical parameters prior to marine isotope stage 13, we suggest a diffusive flux of ions out the top of the sediment column (Schrag et al., 1995) to supply the pore fluid of the overlying sediments. In these sediments, however, planktonic foraminiferal Mg/Ca ratios and high-magnesium calcite presence in the respective sediments show the exclusion of anomalously high Mg/Ca (>6 mmol/mol), when HMC is present.

As diagenetic alteration, especially in such shallow-burial sediments, is controlled by very local conditions and processes, similarities of the planktonic foraminiferal $\delta^{18}O$ and Mg/Ca records SO164–07–4, and M35027 as well as M35053 are remarkable (Fig. 5). The vicinity of these sites to carbonate platforms implies similar processes in sediments with dissolution of significant proportions of aragonite and, most important, high-magnesium calcite, and reprecipitation of low-magnesium calcite.

Acknowledgements. We thank W.-C. Dullo, J. Groeneveld, S. Noe, J. J. G. Reijmer, L. Reuning, and S. Steph for insightful discussions. SEM images were prepared at the Institute for Geosciences, Kiel, with the aid of U. Schuldt and L. Lembke-Jene. We also thank B. Bader, D. Garbe-Schönberg, L. Haxhiaj, J. Heinze, K. Kißling, and S. Koch for laboratory know-how and technical support. P. Mason and G. Nubbe are acknowledged for help with LA-ICP MS analyses. Financial support for this research was provided by the German Ministry of Education and Research (BMBF, project No. 03G0164).

References

Anand, P., Elderfield, H., and Conte, M. H.: Calibration of Mg/Ca thermometry in planktonic foraminifera from sediment trap time series, Paleoceanography, 18(2), 1050, doi:10.1029/2002PA000846, 2003. 2188

Baker, P. A., Gieskes, J. M., and Elderfield, H.: Diagenesis of carbonates in deep-sea sediments: Evidence from Ca/Sr ratios and interstitial dissolved Sr^{2+} data, J. Sediment. Petrol., 52, 71–82, 1982. 2181, 2192

Barker, S., Greaves, M., and Elderfield, H.: A study of cleaning procedures used for foraminiferal Mg/Ca paleothermometry, Geochem. Geophys. Geosys., 4(9), 8407, doi:10.1029/2003GC000559, 2003. 2183, 2189

Bassinot, F. C., Labeyrie, L. D., Vincent, E., Quidelleur, X., Shackleton, N. J., and Lancelot, Y.: The astronomical theory of climate and the age of the Brunhes-Matuyama magnetic reversal, Earth Planet. Sci. Lett., 126, 91–108, 1994. 2184

Bralower, T. J., Fullagar, P. D., Paull, C. K., Dwyer, G. S., and Leckie, R. M.: Mid-Cretaceous strontium-isotope stratigraphy of deep-sea sections, GSA Bull., 109, 1421–1442, 1997. 2192

Carpenter, S. J. and Lohmann, K. C.: Sr/Mg ratios of modern calcite: Empirical indicators of ocean chemistry and precipitation rate, Geochim. Cosmochim. Acta, 56, 1837–1849, 1992. 2192

Crowley, T. J. and Zachos, J. C.: Comparison of zonal temperature profiles for past warm periods, in: Warm Climates in Earth History, edited by: Huber, B. T., MacLeod, K. G., and Wing, S. L., Cambridge University Press, Cambridge, pp. 50–76, doi:10.2277/052164142X, 2000. 2191

Curry, W. B. and Oppo, D. W.: Synchronous, high-frequency oscillations in tropical sea surface temperatures and North Atlantic Deep Water production during the last glacial cycle, Paleoceanography, 12, 1–14, 1997. 2188

Dekens, P. S., Lea, D. W., Pak, D. K., and Spero, H. J.: Core top calibration of Mg/Ca in tropical foraminifera: Refining paleotemperature estimation, Geochem. Geophys. Geosys., 3(4), 1022, doi:10.1029/2001GC000200, 2002. 2180

Droxler, A. W.: Late quaternary glacial cycles in the Bahamian deep basins and in the adjacent Atlantic Ocean, Ph.D. thesis, Miami Univ., Coral Gables, USA, 1984. 2180

Eggins, S., DeDeckker, P., and Marshall, J.: Mg/Ca variation in planktonic foraminifera tests: implications for reconstructing palaeo-seawater temperature and habitat migration, Earth Planet. Sci. Lett., 212, 291–306, 2003. 2181, 2185

Ericson, D. B. and Wollin, G.: Micropaleontological and isotopic determinations of Pleistocene climates, Micropaleontology, 2, 257–270, 1956. 2184

Ericson, D. B. and Wollin, G.: Pleistocene climates and chronology in deep-sea sediments, Science, 162, 1227–1234, 1968. 2184

Frank, T. D. and Bernet, K.: Isotopic signature of burial diagenesis and primary lithological contrasts in periplatform carbonates (Miocene, Great Bahama Bank), Sedimentology, 47, 1119–1134, 2000. 2180

Funk, J. A., von Dobeneck, T., Wagner, T., and Kasten, S.: Late Quaternary Sedimentation and Early Diagenesis in the Equatorial Atlantic Ocean: Patterns, Trends and Processes Deduced from Rock Magnetic and Geochemical Records, in: The South Atlantic in the Late Quaternary: Reconstruction of Material Budgets and Current Systems, edited by: Wefer, G., Mulitza, S., and Ratmeyer, V., pp. 461–497, Springer-Verlag, Berlin, Heidelberg, New York, Tokyo, 2003. 2181

Günther, D., Frischknecht, R., Heinrich, C. A., and Kahlert, H. J.: Capabilities of a 193 nm ArF excimer laser for LA-ICP-MS micro analysis of geological materials, J. Anal. At. Spectrom., 12, 939–944, 1997. 2184

Haak, A. B. and Schlager, W.: Compositional variations in calciturbedites due to sea-level fluctuations, late Quaternary, Bahamas, Int. J. Earth Sci., 78, 477–486, doi:10.1007/BF01776186, 1989. 2193

Haddad, G. A. and Droxler, A. W.: Metastable $CaCO_3$ dissolution at intermediate water depths of the Caribbean and western North Atlantic: Implications form intermediate water circulation during the past 200,000 years, Paleoceanography, 11, 701–716, 1996. 2180

Hastings, D. W., Emerson, S. R., Erez, J., and Nelson, B. R.: Foraminiferal magnesium in *Globigerinoides sacculifer* as a paleotemperature proxy, Paleoceanography, 13, 161–169, 1998. 2188

Hathorne, E. C., Alard, O., James, R. H., and Rogers, N. W.: Determination of intratest variability of trace elements in foraminifera by laser ablation inductively coupled plasma-mass spectrometry, Geochem. Geophys. Geosys., 4, 8408, doi:10.1029/2003GC000539, 2003. 2181

Hover, V. C., Walter, L. M., and Peacor, D. R.: Early marine diagenesis of biogenic aragonite and Mg-calcite: new constraints from high-resolution STEM and AEM analyses of modern platform carbonates, Chem. Geol., 175(3), 221–248, doi:10.1016/S0009-2541(00)00326-0, 2001. 2181

Jansen, H., Zeebe, R. E., and Wolf-Gladrow, D. A.: Modeling the dissolution of settling $CaCO_3$ in the ocean, Global Biogeochem. Cycles, 16, 1027, doi:10.1029/2000GB001279, 2002. 2180

Katz, A.: The interaction of magnesium with calcite during crystal growth at 25–90°C and one atmosphere, Geochem. Cosmochim. Acta, 37, 1563–1586, 1973. 2192

Killingley, J. S.: Effects of diagenetic recrystallization on $^{18}O/^{16}O$ values of deep-sea sediments, Nature, 301, 594–597, 1983. 2181, 2191

Kim, S. T. and O'Neil, J. R.: Equilibrium and nonequilibrium oxygen isotope effects in synthetic carbonates, Geochim. Cosmochim. Acta, 61, 3461–3475, 1997. 2191

Kroon, D., Reijmer, J. J. G., and Rendle, R.: 2. Mid- to Late-Quaternary variations in the oxygen isotope signature of *Globigerinoides ruber* at Site 1006 in the western subtropical Atlantic, in: Proc. ODP, Sci. Results, edited by: Swart, P. K., Eberli, G. P., Malone, M. J., and Sarg, J. F., vol. 166, pp. 13–22, College Station, TX (Ocean Drilling Program), 2000. 2188, 2193

Lohmann, G.: A model for variation in the chemistry of planktonic foraminifera due to secondary calcification and selective dissolution, Paleoceanography, 10, 445–457, 1995. 2180

Lorens, R. B., Williams, D. F., and Bender, M. L.: The early nonstructual chemical diagenesis of foraminiferal calcite, J. Sediment. Petrol., 47, 1602–1609, 1977. 2180

Malone, M. J., Slowey, N. C., and Henderson, G. M.: Early diagenesis of shallow-water periplatform carbonate sediments, leeward margin, Great Bahama Bank (Ocean Drilling Program Leg 166), GSA Bull., 113, 881–894, 2001. 2180

Martinson, D. G., Pisias, N. G., Hays, J. D., Imbrie, J., T. C. More, J., and Shackleton, N. J.: Age dating and the orbital theory of the ice ages: Development of a high-resolution 0 to 300,000-year chronostratigraphy, Quat. Res., 27, 1–29, 1987. 2184, 2204

Mason, P. R. D. and Mank, A. J. G.: Depth-resolved analysis in multi-layered glass and metal materials using laser ablation inductively coupled plasma mass spectrometry (LA-ICP-MS), J. Anal. At. Spectrom., 16, 1381–1388, 2001. 2185

Morse, J. W.: Formation and Diagenesis of Carbonate Sediments, in: Treatise on Geochemistry – The Oceans and Marine Geochemistry, edited by: Mackenzie, F. T., vol. 7, pp. 67–85, Elsevier Ltd., Oxford, 2003. 2181, 2186, 2191, 2193

Mucci, A.: Influence of temperature on the composition of magnesian calcite overgrowths precipitated from seawater, Geochim. Cosmochim. Acta, 51, 1977–1984, 1987. 2192

Mucci, A. and Morse, J. W.: The incorporation of Mg^{2+} and Sr^{2+} into calcite overgrowths: influences of growth rate and solution composition, Geochim. Cosmochim. Acta, 47, 217–233, 1983. 2192

Mulitza, S., Donner, B., Fischer, G., Paul, A., Pätzold, J., Rühlemann, C., and Segl, M.: The South Atlantic Oxygen Isotope Record of Planktic Foraminifera, in: The South Atlantic in the Late Quaternary: Reconstruction of Material Budgets and Current Systems, edited by: Wefer, G., Mulitza, S., and Ratmeyer, V., pp. 121–142, Springer-Verlag, Berlin, Heidelberg, New York, Tokyo, 2004. 2181

Müller, A. (Ed.): Mg/Ca- und Sr/Ca-Verhältnisse in biogenem Carbonat planktischer Foraminiferen und benthischer Ostracoden, vol. 313, Berichte aus dem Institut für Meereskunde, University of Kiel, Germany, 1999. 2181, 2188, 2189, 2207

Mullins, H. T., Wise Jr., S. W., Gardulski, A. F., Hinchey, E. J., Masters, P. M., and Siegel, D. I.: Shallow subsurface diagenesis of Pleistocene periplatform ooze: northern Bahamas, Sedimentology, 32, 473–494, doi:10.1111/j.1365-3091.1985.tb00465.x, 1985. 2191, 2193

Norris, R. D. and Wilson, P. A.: Low-latitude sea-surface temperatures for the mid-Cretaceous and the evolution of planktic foraminifera, Geology, 26, 823–826, 1998. 2181, 2191

Nürnberg, D., Schönfeld, J., Dullo, W.-C., and Rühlemann, C. (Eds.): RV SONNE: Cruise report SO164 RASTA (2002), 109, GEOMAR Report, Kiel, 2003. 2182

O'Neil, J. R., Clayton, R. N., and Mayeda, T. K.: Oxygen isotope fractionation in divalent metal carbonates, J. Chem. Phys., 51, 5547–5558, 1969. 2191

Paillard, D., Labeyrie, L., and Yiou, P.: Macintosh program performs time-series analysis, Eos Trans. AGU, 77, 379, Electronic supplement available at: http://www.agu.org/eos_elec/96097e.html, 1996. 2184

Pearce, N. J. G., Perkins, W. T., Westgate, J. A., Gorton, M. P., Jackson, S. E., Neal, C. R., and Chenery, S. P.: A compilation of new and published major and trace element data for NIST SRM 610 and NIST SRM 612 glass reference materials, Geostandards Newsletter, 21, 115–144, 1997. 2185

Pearson, P. N., Shackleton, N. J., Weedon, G. P., and Hall, M. A.: 29. Multispecies planktonic foraminifer stable isotope stratigraphy through Oligocene/Miocene boundary climatic cycles, Site 926, in: Proc. ODP, Sci. Results, edited by: Shackleton, N. J., Curry, W. B., Richter, C., and Bralower, T. J., vol. 154, pp. 441–449, College Station, TX (Ocean Drilling Program), 1997. 2191

Pearson, P. N., Ditchfield, P. W., Singano, J., Harcourt-Brown, K. G., Nicholas, C. J., Olsson, R. K., Shackleton, N. J., and Hall, M. A.: Warm tropical sea surface temperatures in the Late Cretaceous and Eocene epochs, Nature, 413, 481–487, 2001. 2191

Petschick, R. (Ed.): MacDiff – The user-friendly X-ray powder diffractometry analysis tool for Macintosh computers, available at: http://www.geologie.uni-frankfurt.de/staff/homepages/Petschick/Rainer.html#MacDiff, 2001. 2182

Price, G. D., Sellwood, B. W., Corfield, R. M., Clarke, L., and Cartlidge, J. E.: Isotopic evidence for palaeotemperatures and depth stratification of Middle Cretaceous planktonic foraminifera from the Pacific Ocean, Geol. Mag., 135, 183–191, 1998. 2191

Regenberg, M., Nürnberg, D., Steph, S., Groeneveld, J., Garbe-Schönberg, D., Tiedemann, R., and Dullo, W.-C.: Assessing the dissolution effect on planktonic foraminiferal Mg/Ca ratios: Evidence from Caribbean core-tops, Geochem. Geophys. Geosys., 7, Q07P15, doi:10.1029/2005GC001019, 2006. 2180, 2181, 2183, 2189, 2208

Reichart, G.-J., Jorissen, F., Anschutz, P., and Mason, P. R. D.: Single foraminiferal test chemistry records the marine environment, Geology, 31, 355–358, doi:10.1130/0091-7613(2003)031, 2003. 2181

Rendle, R. H., Reijmer, J. J. G., Kroon, D., and Henderson, G. M.: 6. Mineralogy and sedimentology of the Pleistocene to Holocene on the leeward margin of the Great Bahama Bank, in: Proc. ODP, Sci. Results, edited by: Swart, P. K., Eberli, G. P., Malone, M. J., and Sarg, J. F., vol. 166, pp. 61–76, College Station, TX (Ocean Drilling Program), 2000. 2193

Richter, F. M. and DePaolo, D. J.: Numerical models for diagenesis and the Neogene Sr isotopic evolution of seawater from DSDP Site 590B, Earth Planet. Lett., 83, 27–38, 1987. 2181

Rosenthal, Y., Boyle, E. A., and Slowey, N.: Temperature control on the incorporation of magnesium, strontium, fluorine, and cadmium into benthic foraminiferal shells from Little Bahama Bank: Prospects for thermocline paleoceanography, Geochim. Cosmochim. Acta, 61, 3633–3643, 1997. 2180

Ruddiman, W. F.: Pleistocene sedimentation in the equatorial Atlantic: Stratigraphy and faunal paleoclimatology, Geol. Soc. Am. Bull., 82, 283–302, 1971. 2184

Rudnicki, M. D., Wilson, P. A., and Anderson, W. T.: Numerical models of diagenesis, sediment properties, and pore fluid chemistry on a paleoceanographic transect: Blake Nose, Ocean Drilling Program Leg 171B, Paleoceanography, 16, 563–575, 2001. 2181, 2191

Rühlemann, C., Mulitza, S., Müller, P. J., Wefer, G., and Zahn, R.: Warming of the tropical Atlantic Ocean and slowdown of thermohaline circulation during the last deglaciation, Nature, 402, 511–514, 1999. 2188

Sabine, C. L. and Mackenzie, F. T.: Bank-Derived Carbonate Sediment Transport and Dissolution in the Hawaiian Archipelago, Aquatic Geochem., 1, 189–230, 1995. 2180

Schlitzer, R. (Ed.): Ocean Data View, available at: http://www.awi-bremerhaven.de/GEO/ODV, 2002. 2203

Schmidt, M. W., Spero, H. J., and Lea, D. W.: Links between salinity variation in the Caribbean and North Atlantic thermohaline circulation, Nature, 428, 160–163, 2004. 2188

Schmidt, M. W., Vautravers, M. J., and Spero, H. J.: Western Caribbean sea surface temperatures during the late Quaternary, Geochem. Geophys. Geosys., 7, Q02P10, doi:10.1029/2005GC000957, 2006. 2186, 2187, 2188, 2189, 2206, 2207

Schrag, D. P.: Effects of diagenesis on the isotopic record of late Paleogene tropical sea surface temperatures, Chem. Geol., 161, 215–244, 1999. 2181, 2191

Schrag, D. P., DePaolo, D. J., and Richter, F. M.: Oxygen isotope exchange in a two-layer model of oceanic crust, Earth Planet. Sci. Lett., 111, 305–317, 1992. 2181, 2191, 2193

Schrag, D. P., DePaolo, D. J., and Richter, F. M.: Reconstructing past sea surface temperatures: Correcting for diagenesis of bulk marine carbonate, Geochim. Cosmochim. Acta, 59, 2265–

2278, 1995. 2191, 2193, 2194

Sexton, P. F., Wilson, P. A., and Pearson, P. N.: Microstructual and geochemical perspectives on planktic foraminiferal preservation: “Glassy” versus “Frosty”, Geochem. Geophys. Geosys., 7, Q12P19, doi:10.1029/2006GC001291, 2006. 2181, 2191

Shackleton, N. J., Berger, A., and Peltier, W. R.: An alternative astronomical calibration of the lower Pleistocene timescale based on ODP Site 677, Trans. R. Soc. Edinburgh Earth Sci., 81, 251–261, 1990. 2184, 2204

Slowey, N. C., Wilber, R. J., Haddad, G. A., and Henderson, G. M.: Glacial-to-Holocene sedimentation on the western slope of Great Bahama Bank, Mar. Geol., 185, 165–176, 2002. 2193

Tripati, A. K., Delaney, M. L., Zachos, J. C., and Anderson, L. D.: Tropical sea-surface temperature reconstruction for the early Paleogene using Mg/Ca ratios of planktonic foraminifera, Paleoceanography, 18, 1101, doi:10.1029/2003PA000937, 2003. 2181, 2191

Wade, B. S. and Kroon, D.: Middle Eocene regional climate instability: Evidence from the western North Atlantic, Geology, 30, 1011–1014, 2002. 2191

Wolff, T., Mulitza, S., Arz, H. W., Pätzold, J., and Wefer, G.: Oxygen isotope versus CLIMAP (18 ka) temperatures: A comparison from the tropical Atlantic, Geology, 26, 675–678, 1998. 2188

Table 1. Mass-balanced Mg/Ca and Sr/Ca ratios of an assumed planktonic foraminiferal sample overgrown with diagenetic crystallites. Proportions of overgrowth are given with respect to foraminiferal calcite. Assumed crystallite ratios are obtained from LA-ICP MS results.

Overgrowth	Combined signature of planktonic foraminifera and overgrowth (mmol/mol)				
%	[a]Mg/Ca	[b]Mg/Ca	[c]Mg/Ca	[d]Sr/Ca	[e]Sr/Ca
0	4	4	4	1.4	1.4
5	4.3	4.8	5.8	1.36	1.37
10	4.6	5.6	7.6	1.31	1.34
15	4.9	6.4	9.4	1.27	1.31
20	5.2	7.2	11.2	1.22	1.28

[a] Assumed Mg/Ca (mmol/mol): Planktonic foraminifera = 4; crystallites = 10
[b] Assumed Mg/Ca (mmol/mol): Planktonic foraminifera = 4; crystallites = 20
[c] Assumed Mg/Ca (mmol/mol): Planktonic foraminifera = 4; crystallites = 40
[d] Assumed Sr/Ca (mmol/mol): Planktonic foraminifera = 1.4; crystallites = 0.5
[e] Assumed Sr/Ca (mmol/mol): Planktonic foraminifera = 1.4; crystallites = 0.8

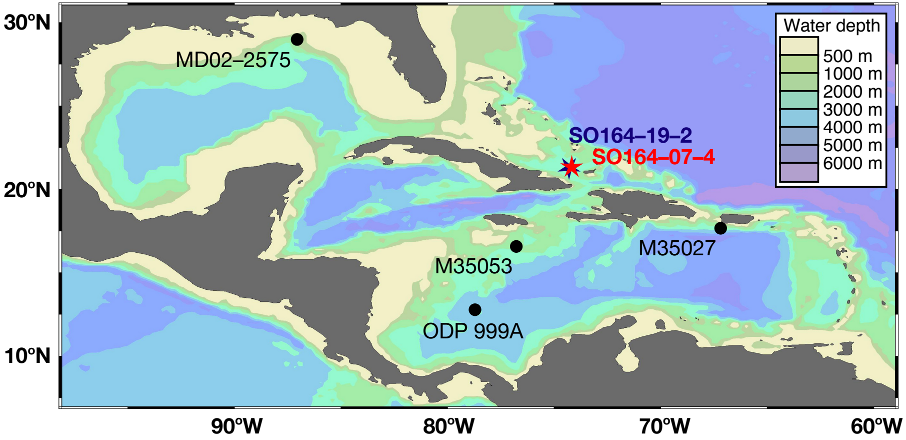

Fig. 1. Bathymetric chart of the Caribbean and the Gulf of Mexico generated with Ocean Data View (Schlitzer, 2002): Stars indicate the site locations of the examined sediment cores SO164–07–4 and SO164–19–2. For comparison, data of sites MD02-2575 (847 m water depth), M35027 (1814 m), M35053 (1698 m), and ODP 999A (2827 m) are shown in this study.

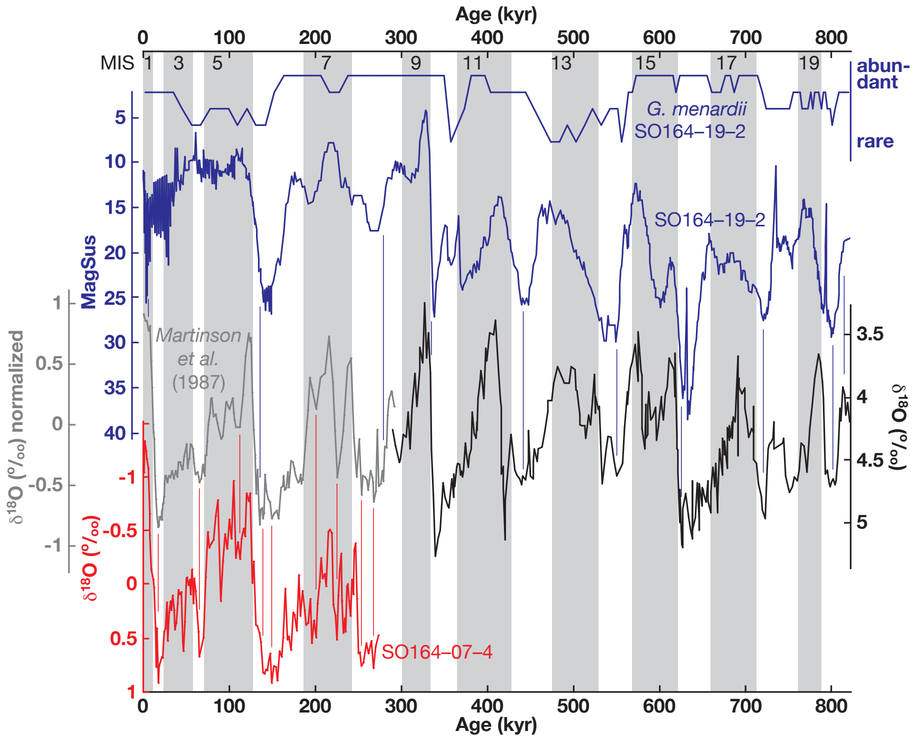

Fig. 2. Stratigraphical framework of sites SO164–07–4 and SO164–19–2 based on the oxygen isotope curve of *G. sacculifer* and the magnetic susceptibility (MagSus) curve, respectively: For graphical correlation back to ~290 ka, the stacked reference curve of Martinson et al. (1987) was used; for the older parts, we used the benthic oxygen isotope record of ODP Site 677 (Shackleton et al., 1990). Tie points are indicated by thin vertical lines. For site SO164–19–2, we additionally estimated the relative abundance of *G. menardii* as indicator of warm isotope stages. Odd numbered marine isotope stages (MIS) are indicated by shading.

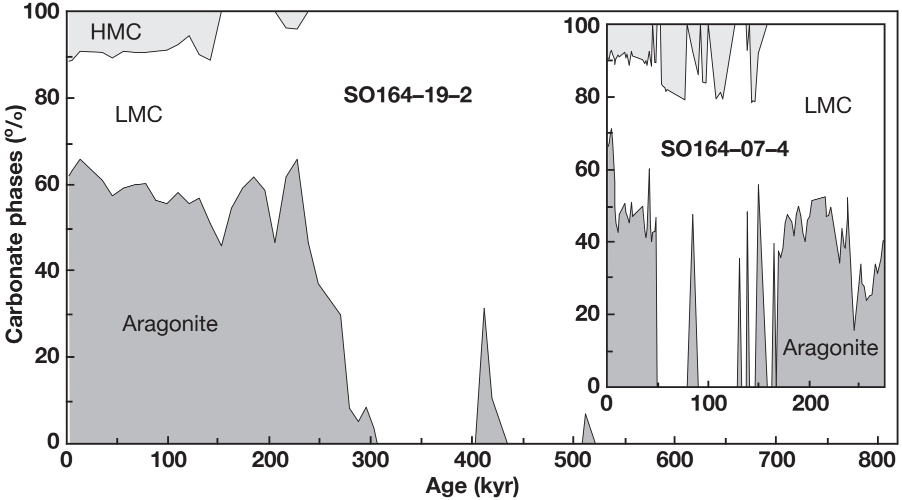

Fig. 3. Carbonate mineralogy of sites SO164–19–2 and SO164–07–4 (inlet) for the last ~820 kyrs and ~270 kyrs, respectively: Proportions of low-magnesium calcite (LMC), high-magnesium calcite (HMC), and aragonite are given in weight %.

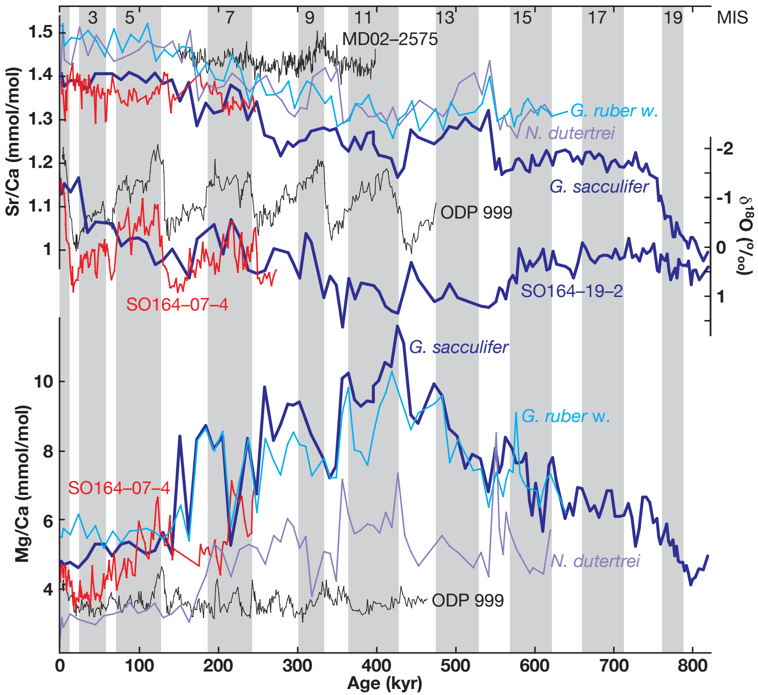

Fig. 4. Sr/Ca and Mg/Ca curves of *G. ruber* w., *G. sacculifer*, and *N. dutertrei* (top and bottom panels, respectively), and the *G. sacculifer* oxygen isotope curve of site SO164–19–2 for the last ~820 kyrs. The trends of the δ^{18}O and Mg/Ca records deviate substantially from Caribbean *G. ruber* w. curves of ODP Site 999 (Schmidt et al., 2006). Likewise, the *G. ruber* w. Sr/Ca ratios are lower than those of *G. ruber* w. of site MD02–2575 from the Gulf of Mexico *Karas and Nürnberg*, pers. comm.), at least prior to MIS 7. Higher resolution *G. sacculifer* curves of site SO164–07–4 follow the atypical trends of site SO164–19–2 records.

Title Page
Abstract
Introduction
Conclusions
References
Tables
Figures
◀▮
▶▮
◀
▶
Back
Close
Full Screen / Esc
Printer-friendly Version
Interactive Discussion

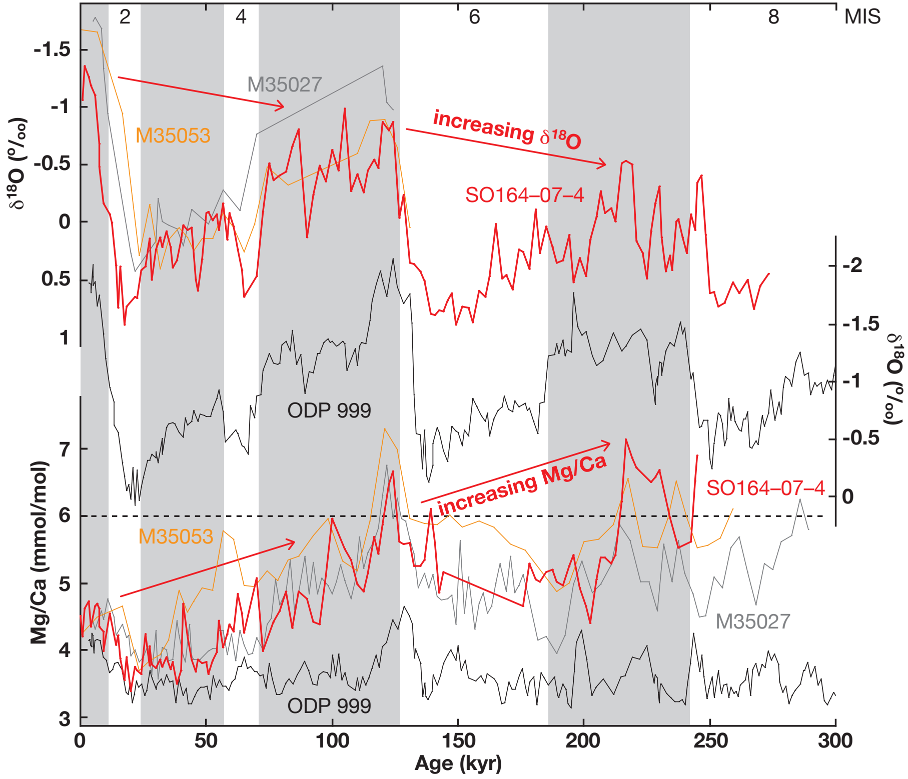

Fig. 5. Oxygen isotope and Mg/Ca curves of *G. sacculifer* of site SO164–07–4 for the last ~250 kyrs: For comparison, Caribbean *G. sacculifer* curves of sites M35027 and M35053 (Müller, 1999), and *G. ruber* w. curves of ODP Site 999 (Schmidt et al., 2006) are given. Increased δ^{18}O and anomalously high Mg/Ca with respect to Holocene values at least during MIS 5 and 7 of sites SO164–07–4, M35027, and M35053 do not follow the expected trend observed for ODP Site 999. Note that Mg/Ca of >6 mmol/mol would convert to open-ocean temperatures of >30.5°C.

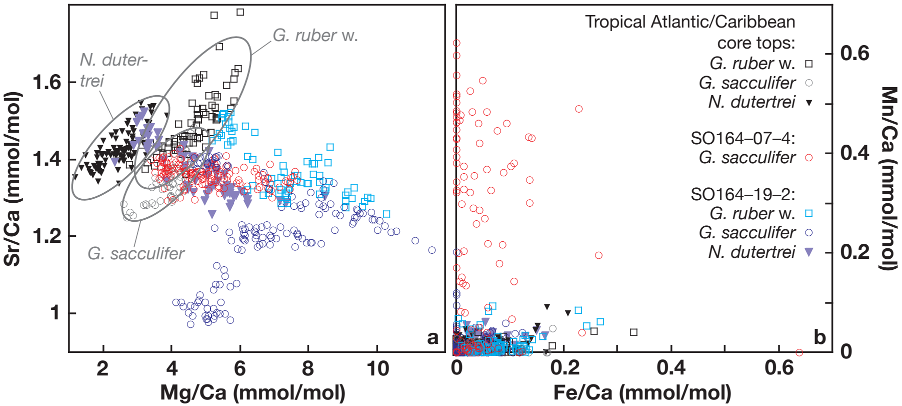

Fig. 6. **(a)** Mg/Ca versus Sr/Ca ratios and **(b)** Fe/Ca versus Mn/Ca ratios of sediment-surface (black and grey symbols) and downcore *G. ruber* w., *G. sacculifer*, and *N. dutertrei* (colored symbols). Marked elliptical areas characterize the modern Mg/Ca and Sr/Ca of tropical Atlantic/Caribbean sediment-surface samples, which resemble open-ocean temperatures of ∼19–28°C (Regenberg et al., 2006, 2007[1]). Related low Fe/Ca (∼0.2 mmol/mol) and Mn/Ca (∼0.1 mmol/mol), unanimously obtained for the core-top foraminifera, indicate that contaminating phases other than carbonate can be neglected as source of Mg^{2+} at least for site SO164–19–2. Annotation of (a) is the same as for (b).

[1] Regenberg, M., Steph, S., Nürnberg, D., Tiedemann, R., and Mulitza, S.: Calibrating Mg/Ca of Multiple Planktonic Foraminiferal Species with δ^{18}O-Calcification Temperatures: Paleothermometry for the Upper Water Column, Earth Planet. Sci. Lett., in review, EPSL-D-06-00991, 2007.

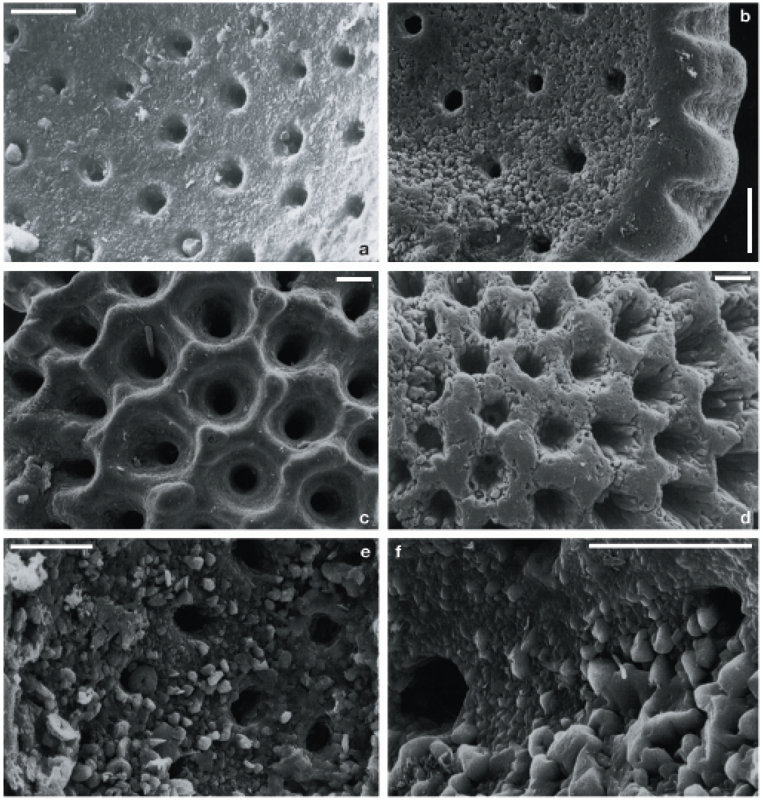

Fig. 7. SEM images of the wall-surface texture of opened planktonic foraminiferal chambers: **(a)** *G. ruber* w. of site SO164–07–4, 118 cm (~23 kyrs), uncleaned; **(b)** *G. ruber* w. of site SO164–19–2, 130 cm (~259.5 kyrs), cleaned; **(c)** *G. sacculifer* of site SO164–07–4, 118 cm (~23 kyrs), cleaned; **(d)** *G. ruber* w. of site SO164–19–2, 260 cm (~473 kyrs), cleaned; **(e)** and **(f)** *N. dutertrei* of site SO164–19–2, 315 cm (~563.5 kyrs), uncleaned and cleaned, respectively. Scale bar = 10 μm.

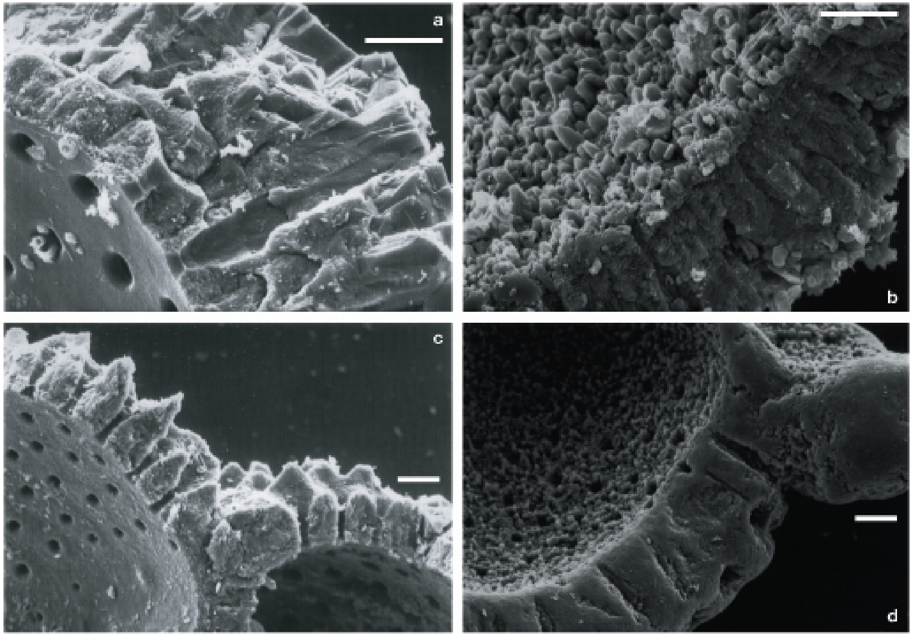

Fig. 8. SEM images of wall-cross sections of opened planktonic foraminiferal chambers: **(a)** *N. dutertrei* of site SO164–07–4, 3 cm (∼0.9 kyrs), uncleaned; **(b)** *G. ruber* w. of site SO164–19–2, 260 cm (∼473 kyrs), uncleaned; **(c)** *G. ruber* w. of site SO164–07–4: 3 cm (∼0.9 kyrs), uncleaned; **(d)** *G. ruber* w. of site SO164–19–2, 260 cm (∼473 kyrs), cleaned. Scale bar = 10 μm.

Title Page
Abstract
Introduction
Conclusions
References
Tables
Figures
◀▌ ▶▌
◀ ▶
Back
Close
Full Screen / Esc
Printer-friendly Version
Interactive Discussion

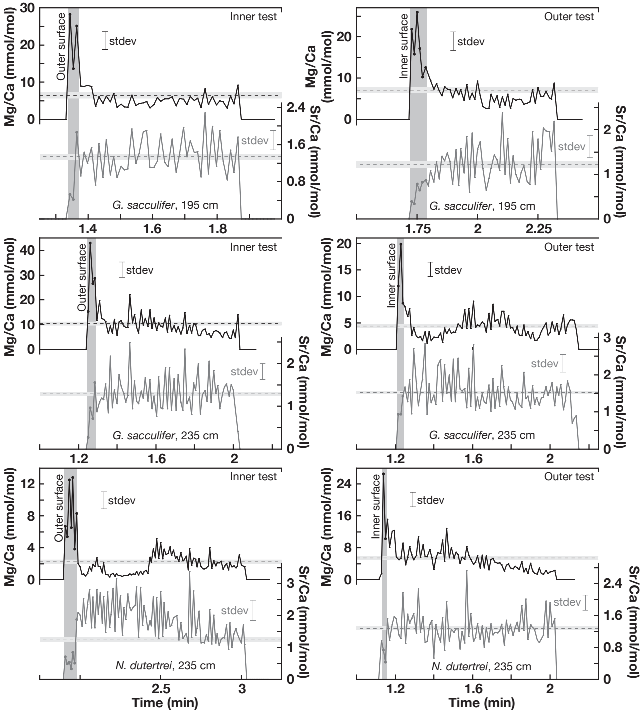

Fig. 9. Time-resolved LA-ICP MS Mg/Ca (upper panels) and Sr/Ca ratios (lower panels) of cleaned foraminiferal samples with diagenetic overgrowths of site SO164–19–2, ablated perpendicular to the chamber-wall surfaces: Sample 195 cm (~365 kyrs), sample 235 cm (~427 kyrs). Standard deviations of single ratios are given as error bars (stdev). Horizontal dashed lines illustrate mean ratios averaged for the entire profile of each plot, standard deviations of the respective means are given as horizontal bars. Vertical grey bars illustrate surface-near ratios revealing elevated Mg/Ca and lowered Sr/Ca compared to the remainder ratios. Left hand profiles are ablated from the outer side of the tests towards the inner side, right hand profiles vice versa.

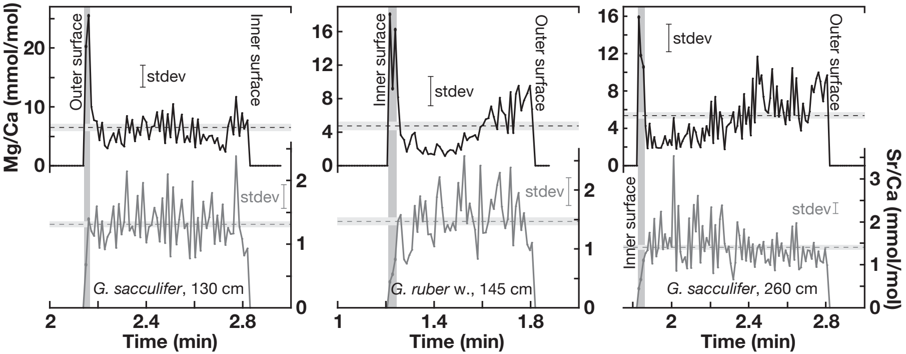

Fig. 10. Time-resolved LA-ICP MS Mg/Ca and Sr/Ca ratios of cleaned foraminiferal samples with diagenetic overgrowths of site SO164–19–2: Sample 130 cm (~260 kyrs), sample 145 cm (~288 kyrs), sample 260 cm (~473 kyrs). For detailed description, see Fig. 9.

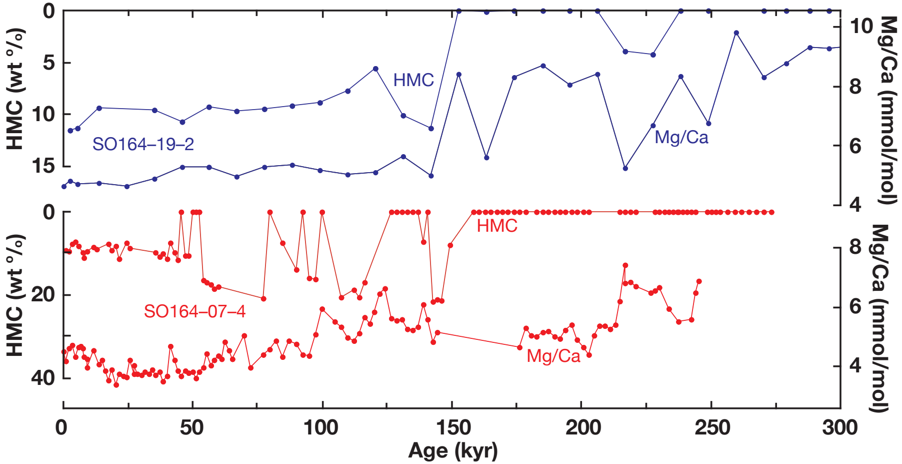

Fig. 11. *G. sacculifer* Mg/Ca ratios and high-magnesium calcite proportion on the carbonate phases of sites SO164–07–4 and SO164–19–2 for the last 300 kyrs: Note that HMC weight percentages are inversely plotted.